Supporting Information

Substrate Protection with Corrosion Scales:

Can we Depend on Iron Carbonate?

Mohammed Al Kindi[1], Gaurav R. Joshi[2], Karyn Cooper[1], Jake Andrews[1], Paulina Arellanes-Lozada[1], Rafael Leiva-Garcia[1], Dirk L. Engelberg[1],

Oier Bikondoa[3,4], Robert Lindsay[1,5]

[1]*Corrosion and Protection Centre, Department of Materials, The University of Manchester, Sackville Street, Manchester M13 9PL, UK*

[2]*IFP Energies Nouvelles (Lyon), Rond-point de l'échangeur de Solaize BP-3, 69360 Solaize, France*

[3]*XMaS-ESRF, 71 Av. Des Martyrs, F-38043 Grenoble Cedex, France*

[4]*Department of Physics, University of Warwick, Gibbet Hill Road, Coventry CV4 7AL, UK*

[5]*Photon Science Institute, The University of Manchester, Manchester, M13 9PL, UK.*

[z]Corresponding author Email Address:

robert.lindsay@manchester.ac.uk

Table S1. List of values employed to determine $CR_{(LPR)}$. R_p+R_s is the resistance determined directly from the gradient of the experimental LPR data. $R_{s(EIS)}$ is the solution resistance, determined from EIS data. G_a is the surface area of the sample exposed to solution. $R_{P(LPR)}$ is the polarisation resistance, corrected for both solution-resistance and sample area (G_a). i_{corr} is the corrosion current density.

$t_{immerse}$ (min)	R_p+R_s (Ω)	$R_{s\ (EIS)}$ (Ω)	G_a (cm^2)	$R_{p\ (LPR)}$ (Ωcm^2)	i_{corr} (mA/cm^2)	$CR_{(LPR)}$ (mmy^{-1})
10	776.0	74	0.785	551.0	6.90E-02	0.803
30	792.3	79	0.785	556.3	6.83E-02	0.788
60	804.5	78	0.785	566.7	6.71E-02	0.779
120	925.2	76	0.785	662.4	5.74E-02	0.666
180	1461.5	68	0.785	1087.2	3.50E-02	0.409
240	3488.0	75	0.785	2662.3	1.43E-02	0.167
300	7036.5	60	0.785	5441.8	6.98E-03	0.082
360	8708.0	67	0.785	6739.6	5.64E-03	0.066
420	10750.0	72	0.785	8329.2	4.56E-03	0.053
480	10840.0	70	0.785	8400.6	4.52E-03	0.053
510	10800.0	68	0.785	8370.7	4.54E-03	0.053
570	10915.0	70	0.785	8459.5	4.49E-03	0.053
618	10980.0	69	0.785	8510.4	4.47E-03	0.052
660	11280.0	68	0.785	8745.3	4.35E-03	0.051

Notes for table:

i_{corr} (mA/cm^2) was determined using:

$$i_{corr} = \frac{B}{R_p}$$

R_p = Solution resistance corrected polarisation resistance (LPR $R_p - R_s$)

B = 38 mV/decade was used for each calculation of i_{corr}.

Corrosion Rate (mm/y) was calculated using:

$$CR = (3.154 \times 10^5) \times \frac{i_{corr} \times M}{F \times z \times \rho}$$

CR: Corrosion Rate (mm/y)
i_{corr}: Corrosion Current Density (mA/cm^2)
M: Molar Mass of metal (55.85 g/mole)
F: Faraday's Constant (96485 C/mole)
Z: Number of electrons exchanged in dissolution reaction (2)
ρ: Metal/Alloy Density (7.8 g/cm^3)

Table S2. Parameter values from best fits to EIS data, using EEC in Figure 4 (a). $\mathbf{R_s}$ and $\mathbf{R_{ct}}$ are ohmic resistors, describing solution resistance ($R_{s(EIS)}$) and charge transfer resistance ($R_{ct(EIS)}$), respectively. $\mathbf{Q_{dl}}$ is a constant phase element, that takes account of the capacitive-like nature of the electrode/solution. $\mathbf{W_d}$ is a finite length Warburg impedance, used to describe limited diffusion (mass transport) across the surface scale. The number of parameters optimised in each fit is also listed, as is the goodness of fit (χ^2).

$t_{immerse}$ (min)	*Circuit Components/Fitting Parameters*						*Number of fit parameters*	χ^2
	$\mathbf{R_s}$	$\mathbf{R_{ct}}$	$\mathbf{Q_{dl}}$		$\mathbf{W_d}$			
	$R_{s(EIS)}$ (Ω)	$R_{ct(EIS)}$ (Ω)	$Y_{Q_{dl}}$ ($\Omega^{-1}s^{\alpha}$)	α	Y_{W_d} ($\Omega^{-1}s^{1/2}$)	B ($s^{1/2}$)		
10	74	621	2.04E-04	0.71	0*	0*	4	3.48E-03
30	79	617	1.79E-04	0.74	0*	0*	4	3.18E-03
60	78	667	1.72E-04	0.74	0*	0*	4	2.00E-03
120	76	842	1.31E-04	0.72	0*	0*	4	6.16E-03
180	68	1391	1.03E-04	0.72	0*	0*	4	2.37E-03
240	75	2479	4.86E-05	0.82	1.21E-03	0.899	6	4.66E-05
300	60	5249	4.30E-05	0.80	7.77E-04	0.836	6	4.41E-04
360	67	4732	3.12E-05	0.84	3.83E-04	1.381	6	1.76E-04
420	72	6047	2.69E-05	0.86	3.21E-04	1.270	6	1.12E-04
480	70	6362	2.58E-05	0.86	3.94E-04	1.480	6	1.53E-04
510	68	6823	2.62E-05	0.86	3.80E-04	1.569	6	3.65E-04
570	70	6449	2.38E-05	0.87	3.20E-04	1.320	6	7.76E-05
618	69	6456	2.34E-05	0.87	3.20E-04	1.320	6	1.19E-04
660	68	6516	2.35E-05	0.87	2.94E-04	1.334	6	1.04E-04

*The fitting parameters for the Warburg impedance element were fixed to a value of 0 during fitting, as optimisation did not improve fit quality.

Notes for table:

Expression for impedance of constant phase element (Z_{CPE}):

$$Z_{CPE} = \frac{1}{Y_{Q_{dl}}(j\omega)^{\alpha}}$$

$Y_{Q_{dl}}$: parameter used to calculate effective capacitance; α: exponent ($0 \leq \alpha \leq 1$ that is a measure of the deviation of Q_{dl} from ideal capacitive behaviour ($\alpha = 1$ for an ideal capacitor); *j*: imaginary unit; ω: radial frequency.

Expression for impedance of finite length Warburg element (Z_{W_d}):

$$Z_{W_d} = \frac{\tanh\left(B\sqrt{(j\omega)}\right)}{Y_{W_d}\sqrt{(j\omega)}}$$

Y_{W_d}: parameter that contains information about diffusion coefficient; B: square root of diffusion time; *j*: imaginary unit; ω: radial frequency

Table S3. Values of C_{dl}, S_a^{rel}, and $CR_{(LPR)}^{S_a corr}$ determined using expressions indicated below; $CR_{(LPR)}$ data from Table S1 are also provided. $CR_{(LPR)}^{S_a corr}$ is the corrosion rate following correction for reduction in electrochemically active surface area as scaling proceeds.

$t_{immerse}$ (min)	C_{dl} (μF)	S_a^{rel}	$CR_{(LPR)}$ (mmy^{-1})	$CR_{(LPR)}^{S_a corr}$ (mmy^{-1})
10	44.8	1.00	0.803	0.80
30	49.0	1.09	0.788	0.72
60	46.3	1.04	0.779	0.75
120	26.7	0.60	0.666	1.11
180	19.3	0.43	0.409	0.95
240	17.5	0.39	0.167	0.43
300	12.2	0.27	0.082	0.30
360	12.5	0.28	0.066	0.24
420	11.9	0.27	0.053	0.20
480	11.7	0.26	0.053	0.20
510	11.4	0.26	0.053	0.20
570	11.8	0.26	0.053	0.20
618	11.7	0.26	0.052	0.20
660	11.7	0.26	0.051	0.20

Notes for table:
Expression from Brug *et al*.[22] used to calculate C_{dl}:

$$C_{dl} = \left[Y_{Q_{dl}} \left(\frac{1}{R_{s(EIS)}} + \frac{1}{R_{ct(EIS)}} \right)^{(\alpha - 1)} \right]^{\left(1/\alpha\right)}$$

Values of $Y_{Q_{dl}}$, $R_{s(EIS)}$, $R_{CT(EIS)}$, and α were obtained from Table S2.

Expression used to calculate S_a^{rel}:

$$S_a^{rel} = \frac{C_{dl}(t)}{C_{dl}(10)}$$

It is assumed that $C_{dl}(10) \approx C_{dl}(0)$, as there is no appreciable surface scale at $t_{immerse}$ = 10 min.

Expression used to calculate $CR_{(LPR)}^{S_a corr}$:

$$CR_{(LPR)}^{S_a corr} = \frac{CR_{(LPR)}}{S_a^{rel}}$$

Table S4. Values of S_a^{rel}, $R_{\delta(EIS)}$, $R_{\delta(EIS)}^{S_a corr}$, $R_{ct(EIS),}$ and $R_{ct(EIS)}^{S_a corr}$; $R_{\delta(EIS)}$, $R_{\delta(EIS)}^{S_a corr}$, and $R_{ct(EIS)}^{S_a corr}$ were determined using expressions indicated below. To demonstrate the agreement between LPR and EIS data, $CR_{(EIS)}^{S_a corr}$ and $CR_{(LPR)}^{S_a corr}$ are listed in the final two columns, where the former is calculated using the sum of $R_{ct(EIS)}$ and $R_{\delta(EIS)}$.

$t_{immerse}$ (min)	S_a^{rel}	$R_{\delta(EIS)}$ (Ω)	$R_{\delta(EIS)}^{S_a corr}$ (Ω)	$R_{ct(EIS)}$ (Ω)	$R_{ct(EIS)}^{S_a corr}$ (Ω)	$CR_{(EIS)}^{S_a corr}$ (mmy^{-1})	$CR_{(LPR)}^{S_a corr}$ (mmy^{-1})
10	1.00	0	0	621	621.0	0.91	0.80
30	1.09	0	0	617	674.7	0.84	0.72
60	1.04	0	0	667	690.4	0.82	0.75
120	0.60	0	0	842	502.7	1.13	1.11
180	0.43	0	0	1391	600.4	0.94	0.95
240	0.39	741.2	339.3	2479	971.6	0.45	0.43
300	0.27	1074.8	334.3	5249	1429.6	0.33	0.30
360	0.28	3602.0	1213.4	4732	1320.2	0.24	0.24
420	0.27	3951.5	1088.8	6047	1614.0	0.21	0.20
480	0.26	3756.3	1002.3	6362	1666.7	0.21	0.20
510	0.26	4125.3	1052.0	6823	1743.9	0.20	0.20
570	0.26	4124.4	1079.5	6449	1699.2	0.20	0.20
618	0.26	4121.4	1087.0	6456	1686.3	0.21	0.20
660	0.26	4541.3	1186.2	6516	1702.6	0.20	0.20

Notes for table:

Expression used to calculate $R_{\delta(EIS)}$:

$$R^{\delta(EIS)} = \left(\frac{1}{\sqrt{2}Y_{W_d}}\right)B^{1/2}$$

Values of Y_{W_d} and B were obtained from Table S2.

Expressions used to calculate $R_{\delta(EIS)}^{S_a corr}$ and $R_{ct(EIS)}^{S_a corr}$:

$$R_{\delta(EIS)}^{S_a corr} = R_{\delta(EIS)} \times S_a^{rel}$$

and

$$R_{ct(EIS)}^{S_a corr} = R_{ct(EIS)} \times S_a^{rel}$$

Experimental Details

Substrate Composition and Microstructure

Typical impurities and their ppm concentrations in the Fe substrates (Purity: 99.99+%; Supplier: Goodfellow) employed in this study are listed in Table S5. Figure S1 shows a SEM image of the typical microstructure exhibited by these samples following the specified heat treatment.

Table S5. Typical impurities and their ppm concentrations in the Fe substrates (Purity: 99.99+%; Supplier: Goodfellow) used in this study.

Impurity	Concentration (ppm)
Al	1.6
Cr	6.6
Boron	0.77
Cobalt	12
Copper	2.1
Ga	0.7
Germanium	6.2
Manganese	4.1
Mo	0.36
Ni	2.8
Phosphorous	7.2
Tantalum	1
Tin	0.15
Titanium	1.4
Tungsten	0.15
Zinc	0.3

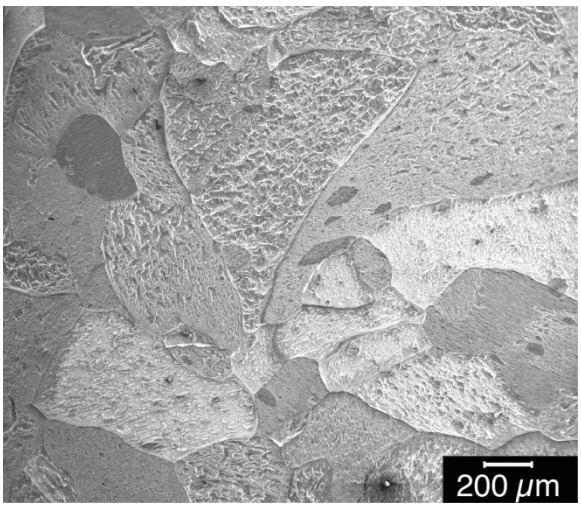

Figure S1. SEM image of heated treated Fe sample, which has been etched in 2% Nital solution to reveal the microstructure.

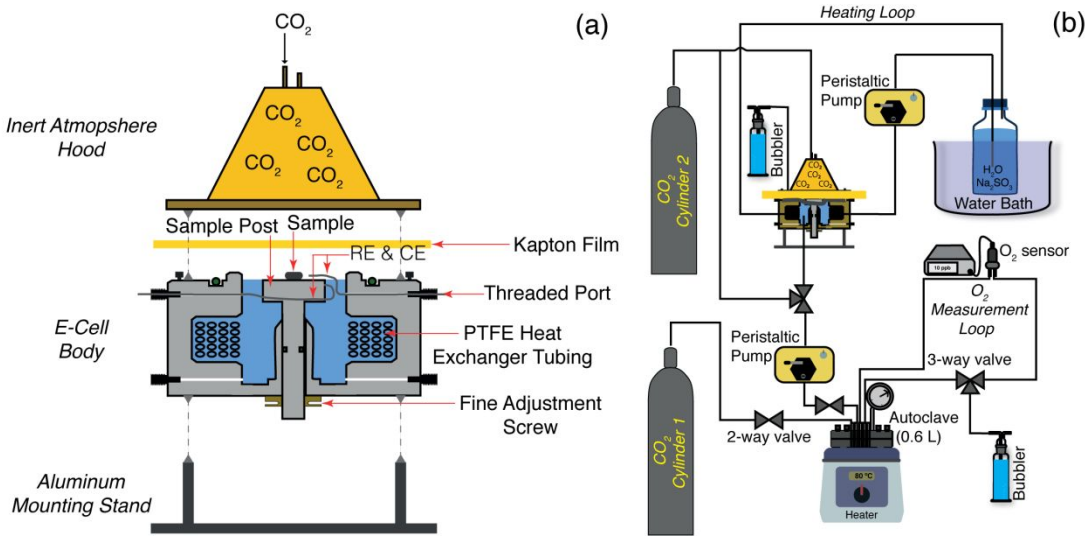

Figure S2. (a) Schematic diagram of the three distinct elements of the E-cell used in this study, i.e. mounting stand, E-cell body, and inert atmosphere hood. Various components are labelled. (b) Schematic diagram of the experimental setup associated with the E-cell, including autoclave for sweet solution preparation, *Heating Loop*, *O_2 Measurement Loop*, and CO_2 cylinders.

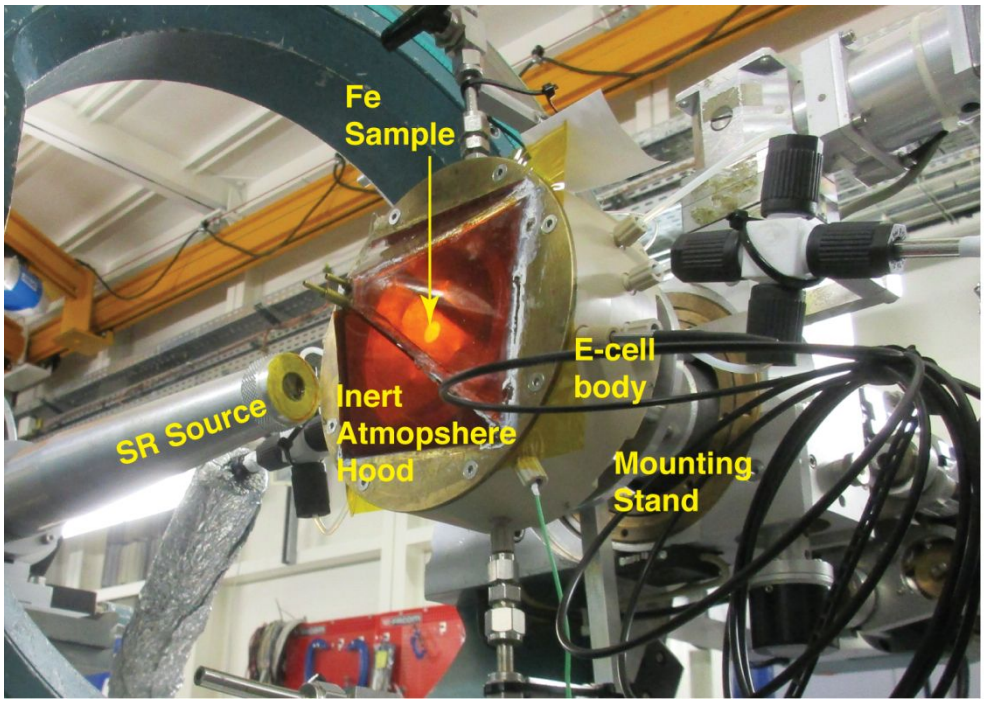

Figure S3. E-cell mounted on BM28 diffractometer at the ESRF. The three distinct elements of the E-cell are indicated: mounting stand, E-cell body and inert atmosphere hood. It should be noted that the E-cell is mounted so that the sample plane is oriented vertically to avoid trapping gas bubbles (e.g. H_2 from cathodic reaction) between the sample surface and Kapton film.

E-cell Details

As illustrated in Figure S3 (and Figure S2 (a)), the E-cell comprises three distinct elements: a mounting stand, E-cell body, and inert atmosphere hood. The mounting stand, fabricated from aluminium, is employed to attach the E-cell to the diffractometer on BM28. Concerning the E-cell body, it is manufactured from polyether ether ketone (PEEK), and has 11 threaded ports penetrating its side wall. Reference and counter electrodes (both Pt wires) are inserted through two of these ports for electrochemical measurements. Another three ports are used as *sweet* solution inlet/outlet, and for the insertion of a type-K thermocouple. The final six ports are occupied by 3 sets of polytetrafluorethene (PTFE) coiled tubing (3 mm outer dimeter, and each ~ 3500 mm in length), which are used as a heater exchanger to enable the temperature in the E-cell to be raised from room temperature to a maximum of ~ 80°C. Water of the desired temperature is flowed through these coils, using a thermostatically controlled water bath. The sample (working electrode) is mounted on a central polyvinylidene (PVDF) post, which can be translated relative to the main body; fine tuning of the post/sample position is achieved with an adjustment screw located beneath the cell.

X-rays enter/exit the E-cell, and impinge on the sample, through a Kapton film (thickness = 25.4 μm) located above the sample. This film is sealed to the E-cell to avoid solution leakage. As depicted in Figure S3, the depth of the solution above the sample can be controlled by either moving the PVDF post or inflating/deflating the Kapton film by adding/removing solution; the two measurement geometries are referred to as thin-film and thick-film. A Kapton-windowed (thickness = 127 μm) inert atmosphere hood, fabricated from brass, is secured atop the Kapton film with a Viton O-ring. During an experiment, CO_2 is continuously flowed through the hood to avoid O_2 permeating through the Kapton film and dissolving in the sweet solution in the E-cell.

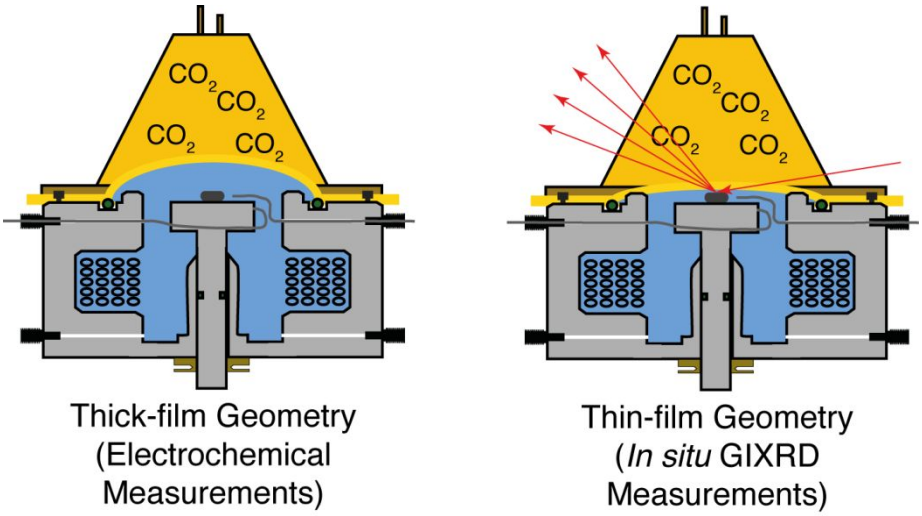

Figure S4. Illustration of thick-film and thin-film E-cell geometries, employed for electrochemical and *in situ* GIXRD measurements, respectively.